DRAFT VERSION JANUARY 24, 2019

Typeset using IATEX **two-column** style in AASTeX62

Multiple Populations of Extrasolar Gas Giants

Comment [Editor1]: Remark: The font was changed for ease of editing.

SHOHEI GODA[1] AND TARO MATSUO[1]

[1] Department of Earth and Space Science, Graduate School of Science, Osaka University, 1-1, Machikaneyamacho, Toyonaka, Osaka
560-0043, Japan

ABSTRACT

There are two planetary formation scenarios: core accretion and gravitational disk instability. ~~Most extrasolar gaseous objects discovered to date are thought to be formed from the core accretion, based~~Based on ~~a~~the fact that gaseous objects are preferentially observed around metal-rich host stars~~.~~, most extrasolar gaseous objects discovered to date are thought to have been formed by core accretion. Here, we present ~~the~~ 623 samples ~~in 520 planetary systems comprising~~of gaseous planets and brown dwarfs ~~discovered~~found in 520 planetary systems. Discovered by radial-velocity measurements ~~in~~, they span three mass regimes, with boundary values ~~of~~at 4 and 20 Jupiter ~~mass in terms of~~ masses. We have performed cluster analyses of these samples regarding the host-star metallicity ~~through performing a cluster analysis to the samples,~~, after minimizing ~~an~~ the impact of the radial-velocity selection effect ~~of radial velocity measurements~~ on the cluster analysis. The larger ~~boundary~~ mass is thought to be ~~a~~ the boundary between ~~planet~~ planetary and ~~sub-stellar formations~~ substellar formation around G-type stars ~~, being in agreement~~; it agrees with the upper mass limit ~~of the~~for core-accreted planets predicted by some theoretical studies. The distributions of ~~host-star metallicities,~~the masses and eccentricities ~~for the~~of planetary objects lighter than 20 Jupiter ~~mass orbiting~~ masses that orbit G-type stars as functions of the host-star metallicities can be explained naturally ~~explained~~ by the core-accretion model. In contrast, the lower mass ~~limit reflects a~~appears to reflect the difference between planetary formation processes around early-type and G-type stars. A population with masses ~~ranging from~~between 4 ~~to~~and 20 Jupiter ~~mass orbiting~~ masses that orbits early-type stars is thought to ~~be composed~~consist of planets formed *via* the gravitational disk instability, ~~considering~~because that ~~the~~ population ~~preferably~~preferentially orbits metal-poor stars or is independent of the host-star metallicity.

Keywords: methods: data analysis - planets and satellites: terrestrial planets

1. INTRODUCTION

~~Decades ago, the~~

The discussion of planetary formation ~~in solar system~~ was developed decades ago for the solar system (Hayashi *et al*. 1985). Two representative formation scenarios for Jupiter have been proposed: ~~Core~~core accretion (Perri & Cameron 1974; Mizuno 1980; Pollack *et al.* 1996) and disk instability (Kuiper 1951; Boss 1997; Mayer *et al*. 2002). In theory, the two ~~planetary~~ planet-formation processes have different dependences on the proto-planetary-disk metallicity~~, which is~~ —defined as the ratio of the ~~metal~~ number-density of metals to hydrogen atoms~~,~~—and ~~planet~~on the planetary mass (*e.g.,* Matsuo *et al.* 2007). ~~For~~In the core-accretion model, a ~~proto-planet~~protoplanet core easily grows to the critical core mass before the disk gas dissipates. This occurs because the disk ~~metallic-ity~~metallicity reflects the building materials available for the core (Ida & Lin 20046; Mordasini *et al*. 2012). In fact, since the first planet orbiting a normal star was discovered (Mayor & Queloz 1995), large-sized radial-velocity observations have revealed that, ~~while~~although the metallicities of stars hosting smaller planets—such as Neptune-like planets and super-Earths—are significantly lower than those of stars orbited by extrasolar gas giants (Mayor *et al*. 2011; Wang & Fischer 2015), the gas giants preferentially orbit metal-rich stars (*e.g*., Santos *et al.* 2003; Fischer & Valenti 2005). Because the central star and its surrounding protoplanetary ~~disks~~disk are formed from ~~a~~the same molecular cloud, according to the primordial hypothesis, most gas giants are thought to have formed *via* ~~the~~ core accretion. ~~Regarding the planet mass, the~~Indeed, gas giants with ~~planet mass~~ planetary masses up to 30 ~~Mj~~M_J are potentially formed *via* ~~the~~ core accretion (*e.g*., Tanigawa & Ikoma 2007; Tanigawa & Tanaka 2016), where ~~Mj~~M_J represents the Jupiter mass. The number of ~~the~~ gas giants more massive than a few ~~Mj~~M_J gradually decreases as the ~~planet~~planetary mass ~~is larger~~increases (*e.g*., Mordasini *et al*. 2009).

For the disk-instability scenario, the relationship between disk metallicity and disk-instability-induced planetary formation has been studied theoretically~~studied; there exists~~. There are reports of a negative correlation (Cai *et al*. 2006; Durisen *et al*. 2007), a very weak positive correlation (Mayer *et al*. 2007), and no correlation (Boss 2002) ~~in~~with the ~~metallicity range~~metallicities of the stars hosting the observed planets. Although ~~the~~a lower limit may exist on the masses of ~~the~~ disk-instability-induced planets ~~may exist~~ (Matsuo *et al*. 2007), the mass distribution of ~~the~~ gas giants formed *via* the disk instability still remains an open question. On the other hand, direct imaging of the extrasolar planets orbiting HR8799, Formalhaut, and beta Pictoris ~~reported in 2008 and 2010~~ (Marois *et al*. 2008; Kalas *et al*. 2008; Lagrange *et al*. 2010~~), respectively,~~) has confirmed the ~~existing~~existence of outer planets, which can be ~~naturally~~ explained better by the disk-instability scenario rather than ~~the~~by extended core accretion with migration or planet-planet scattering (Dodson-Robinson *et al*. 2009). Thus, ~~there may exist~~ two populations of planets that have originated from the two ~~planetary formations.~~different planet-formation mechanisms may exist.

Several previous studies (Ribas & Miralda-Escude 2007; Santos *et al*. 2017) ~~showed~~have shown that the gas giants are divided into two regimes ~~with~~separated by a boundary mass of 4 ~~Mj~~M_J, and they have interpreted the two populations as ~~an outcome originated~~outcomes originating from the two planetary-~~formations; while the~~ -formation mechanisms: gas giants lighter than 4 ~~Mj~~M_J are core-accreted planets, ~~the gas giants~~while those more massive than 4 ~~Mj~~M_J are formed through the disk instability. ~~In addition~~In contrast, by performing a cluster analysis on the diagram of planetary mass *vs*. host-star metallicity and, Schlaufman (2018) found ~~that there is~~ a transition between 4 and 10 ~~Mj~~M_J instead of a clear boundary ~~of~~at 4 ~~Mj~~M_J for gaseous objects orbiting G-type stars~~, performing a cluster analysis to a diagram of host-star metallicity and planet mass.~~. However, in theory, it is possible to form very massive gas giants—up to 30 ~~Mj~~ M_J—*via* ~~the~~ core accretion ~~in theory (e.g., Tani-gawa~~(*cf*., Tanigawa & Ikoma 2007; Mordasini *et al*. 2009; Tanigawa & Tanaka 2016~~)~~), and the upper mass limit ~~of the~~for core-accreted planets is also expected to depend on the disk metallicity (Mordasini *et al*. 2012). ~~Pebble~~Recently, pebble accretion has been ~~recently~~ proposed as ~~the~~a third planetary-formation scenario ~~that~~; it enables massive ~~core~~cores to be formed in the outer ~~region~~regions of a planetary system beyond 10 AU (Ormel & Klahr 2010; Lambrechts & Johansen 2012~~);~~). Planets more massive ~~planets~~ than ~~the core-accreted planets are~~those that can be formed by core accretion can potentially be formed thanks to a ~~wider hill~~larger Hill radius in ~~more~~ the outer ~~region.~~regions. Thus, it is still unknown whether ~~the~~a boundary mass of 4 ~~Mj~~ M_J—or ~~the~~a transition between 4 and 10 ~~Mj~~ M_J—can be applied as the upper ~~boundaries~~boundary of ~~the~~a bottom-up planetary-formation ~~scenarios~~scenario such as ~~the~~ core accretion, ~~and~~or whether pebble accretion ~~is still unknown.~~applies instead. Furthermore, although ~~the~~ previous studies ~~did~~have not ~~consider the~~considered selection effects ~~of the~~on planet detections, the detection limits ~~of~~for the radial-velocity measurements clearly depend on the metallicity of the host star ~~(~~[see Figure 1 (a~~)).~~)].

Comment [Editor2]: Remark: This should be capitalized if it is a proper name.

Here, we report ~~that~~ on 623 samples ~~comprising~~ of gaseous planets and brown-dwarfs ~~are~~, which we have divided into three-mass regimes ~~with~~ separated by boundary masses ~~of~~ at 4 and 20 ~~Mj.~~M_J. The upper boundary mass is thought to represent the upper mass ~~limits of~~ limit for planetary objects that can be formed around G-type and early-type stars. The lower boundary mass represents ~~a~~ the difference between the planetary~~-~~-formation processes around G-type and early-type stars. While most of the samples orbiting ~~the~~ G-type stars are naturally explained by the core~~-~~-accretion model, the samples more massive than 4 ~~Mj orbiting~~M_J that orbit early-type stars seem to be formed by the disk~~-~~-instability process~~, where the~~. In this paper, we define G-type and early-type stars ~~were defined~~ as ~~stars~~those with masses ranging from 0.8 to 1.3 ~~Solar mass, M☉,~~solar masses ($M_\odot$) and those more ~~larger~~massive than 1.3 ~~M☉ in this paper~~$M_\odot$, respectively. Note that ~~the samples~~ we have constructed the samples used for this study ~~were considered such~~so that ~~an~~ the impact of ~~the selection effect of the~~ radial~~-~~-velocity selection effects on the statistical analysis ~~is~~ are minimized.

This paper is organized as follows. In Section 2, first, we explain how we constructed the samples ~~applying to~~ used for our statistical ~~analysis were constructed~~analyses, introducing the "common-biased samples~~"~~ ~~that were~~," which we have selected ~~such that an~~ to minimize the impact of the difference between ~~the~~ selection effects in ~~the~~ metal-rich and -poor regions on the ~~analysis is minimized.~~analyses. In Section 3, we derive the boundary metallicity that ~~is divided~~ divides the samples into two regions ~~such that~~for which the distributions of ~~the planet~~planetary masses and semi-major axes ~~are most different. We~~differ the most. By applying a Gaussian-mixture model, we also show that the samples are divided into three~~-~~ mass regimes ~~through applying the Gaussian mixture model to the samples and three-mass regimes~~, which arise from the difference between the distributions ~~for~~of gaseous objects orbiting G-type and early-type stars. In Section 4, by comparing the results of our statistical analysis with the two planetary-formation models, we discuss ~~what~~ the upper~~-~~ mass limit ~~of the~~for gas giants formed *via* ~~the~~ bottom-up planetary formation ~~is~~, and we consider whether ~~the~~ disk-instability-induced planetary formation occurs~~, comparing the results of the statistical analysis with the two planetary formation models~~.

2. METHOD

In this section, we explain how to perform statistical ~~analysis~~analyses for extrasolar gaseous objects to understand their formation and evolution processes, and we show how to deal with the selection effect of the radial~~-~~-velocity measurements by which the samples ~~constructed~~used for this study were detected. We also explain how we constructed the samples we used, determining the boundary between gas dwarfs~~-~~---such as Neptune-like planets~~-~~—and gaseous giants.

2.1. ~~–~~*Overview of the Statistical Analysis*

In this study, ~~we~~ first, we examined whether the difference between the distributions of semi-major axes and masses for gaseous objects orbiting metal-rich and -poor stars arises from ~~the~~ radial-velocity selection ~~effect of radial velocity measurements~~effects or ~~from~~whether it is due to the dependence of the planetary formation and evolution ~~process~~processes on ~~the~~ disk ~~metal-licity, constructing~~metallicity. We have constructed samples ~~named as~~that we term "common-biased samples~~" that~~," which minimize ~~an~~ the impact of the selection ~~effect~~effects on the distributions, as ~~to be discussed~~we discuss in Section 2.2. Given that ~~the~~ measurement errors follow a normal distribution, we have sampled the host-star metallicities and companion masses, and then divided the common

-

biased samples into two ~~by a~~groups that depend upon the host-star metallicity. Using the "anderson_ksamp" module in Python, we have compared the planetary masses and semi-major axes of the divided sub-samples ~~in terms of planet mass and semi-major axis with~~ using the two-sample Anderson-Darling test. ~~Calculating~~By calculating the p-values derived from ~~the two-sample Anderson-Darling~~that test as a function of the host-star metallicity, we searched for a boundary ~~metallic-ity~~metallicity that divides the common-biased samples ~~such~~so that the distributions of companion masses and semi-major axes for the two sub-samples are the most different. We iterated this procedure 1,000 times and finally evaluated how~~-much~~ different the distributions of the two common-biased sub-samples are in terms of the semi-major axis and planet mass at the boundary metallicity. ~~This result is shown in~~ Section 3.1 shows this result.

Next, we explored how many populations exist in ~~ex-trasolar~~the extrasolar gaseous objects discovered so far, to investigate ~~what~~ the upper mass limit ~~of the~~for core-accreted planets~~ is;~~. In particular, we have re-examined whether ~~only~~there are just two populations ~~exist in the~~of extrasolar gaseous objects, as ~~shown~~has been found in ~~the~~ several previous studies (Ribas & Miralda-Escude 2007; Santos *et al.* 2017; Schlaufman 2018). Using the "~~GaussianMix-ture~~Gaussian_Mixture" package in Python, we applied a two-dimensional Gaussian~~ ~~-mixture model to the diagram of companion masses *versus* host-star metallicities ~~versus companion masses~~ for the common-biased samples. ~~The number of the~~We used from one to ten Gaussian~~ ~~-mixture models ~~used~~ for this cluster analysis~~ ranges from 1 to 10.~~. We determined the number of ~~the~~ components of the best Gaussian~~ ~~-mixture model based on the Bayesian Information Criterion, as well as on the cluster to which ~~cluster~~ each common-biased sample ~~belong.~~belongs. Sampling the host-star metallicities and companion masses, we repeated this procedure 1,000 times. ~~This result is introduced in~~ Section 3.3 shows this result.

Comment [Editor3]: Remark: Is this named correctly? Please check.

Comment [Editor4]: Remark: It is common practice to list the quantity plotted on the y-axis first, as a function of the quantity plotted on the x-axis. We have changed this order throughout the manuscript to be consistent with this practice.

2.2. —*Common-biased Samples*

~~In order to reveal~~

To determine the distributions of masses and orbital properties for samples orbiting ~~various~~ host-star of various metallicities, we ~~gathered~~collected extrasolar gaseous objects that have been discovered by radial~~ ~~-velocity observations ~~that can precisely determine~~ for which the lower limit of companion mass, the semi-major axis, and the eccentricity~~. The gathered~~ can be determined precisely. We term these objects ~~were referred to as~~ the "original samples~~" in this paper. Considering that~~." Because there ~~exists the~~is a relation between the planetary-formation processes and the host-star metallicity, as ~~introduced~~discussed in Section 1, it is preferable that the accuracies and durations (or "terms") of the radial~~ ~~-velocity measurements~~, which detected~~ used to detect the original samples~~, are~~ be independent of the host-star metallicity. ~~This is because the~~ The original samples detected *via* radial~~ ~~-velocity measurements are influenced by two selection effects: (i) limited sensitivity to long-period planets, owing to the relatively short observation terms and (ii) limited sensitivity to low-mass planets, owing to ~~a lack of measurement~~insufficient precision in the radial~~-~~-velocity ~~measurement.~~measurements. The maximum semi-major axis~~,~~ $a\backslash_{max}$ ~~,~~and the lower mass limit~~,~~ M_p sin $i\backslash_{min}$~~,~~ of ~~the~~a detectable companion can be determined by the accuracy~~, a,~~ σ and the term~~, τ,~~ τ of the radial~~-~~-velocity measurements ~~as below~~ (Torres *et al.* 2008~~),~~):

$$a|_{max} = M_*^{\frac{1}{3}}\tau^{\frac{2}{3}}, \quad (1)$$

$$M_p \sin i|_{min} \approx 4.919 \times 10^{-3} P^{\frac{1}{3}}(1-e^2)^{\frac{1}{2}} M_*^{\frac{2}{3}}\sigma, \quad (2)$$

where, M~~,,,,~~*, P, e, and i are, respectively, the host-star mass, and the orbital period, eccentricity, and orbital inclination of the companion~~, respectively. The~~. We have derived the region in which a companion can be detected ~~was derived~~ for each radial~~-~~-velocity measurement based on ~~Equation~~Equations (1) and (2). Figure 1 (a) compares the detection probabilities ~~of~~ for a companion ~~with~~against the radial~~-~~-velocity measurements ~~of~~ for all of the samples, for just the early-type stars, and for the G-type stars~~ in the~~, for both metal-rich and ~~-~~–poor ~~regions~~cases, plotted in terms of the semi-major axis and the lower mass limit. Note that we have fixed the boundary metallicity ~~was fixed~~for this figure to be 0 dex. As shown in Figure 1, the accuracies of the radial~~-~~-velocity measurements for the original metal-poor ~~original~~ samples are clearly worse than those for the metal-rich ones. The detectable semi-major axes for the original samples orbiting ~~the~~ metal-rich stars are almost same as those ~~of~~for the metal-poor samples. Thus, the ~~selection effect of the~~ radial~~-~~-velocity ~~measurements~~selection effect depends on the host-star metallicity and affects the distributions of masses and semi-major axes for the two original sub-samples orbiting the metal-rich and -poor samples.

Focusing on ~~a~~the fact that the distributions of masses and semi-major axes for the original samples discovered in the metal-rich (-poor) region are biased ~~with the selection effect of~~due to the radial~~-~~-velocity ~~measurements~~selection criteria for the metal-rich (-poor) stars, we can minimize the impact on the original samples of the difference between the selection effects ~~in~~for the metal-rich and -poor ~~regions on the original samples through~~cases by filtering the metal-rich (-poor) original samples with the selection ~~effect in~~criteria for the metal-poor (-rich~~). The~~) samples. This equalizes the selection biases ~~of~~for the samples orbiting the metal-rich and -poor stars ~~were equalized (~~[see Figure 1 (b~~))~~.)]. In the filtering process, we judged whether each original sample~~ simply~~ satisfies the following criteria:

$$M_{p,j} \sin i_j - M_{p,k} \sin i_k|_{min} \geq \frac{1}{2}(a_j - a_k|_{max}), \quad (3)$$

$$a_j \leq a_k|_{max}, \quad (4)$$

Comment [Editor5]: Tip: Hyphenation of Compound Adjectives: For the ease of readability and comprehension, hyphenation may be used to link the components of compound adjectives that precede the nouns they modify. In this case, the noun "measurements" is modified by the compound adjective "radial, velocity" which may be hyphenated.

Comment [Editor6]: Remark: It is not clear how this is shown by Fig. 1. Please clarify.

Comment [Editor7]: Remark: Should this be “regions” or “cases”? Please check.

where j and k represent the j-th original sample and the k-th radial velocity observation, respectively. Note that the *j*-th original sample is observed by ~~the~~a randomly selected *k*-th radial ~~-~~-velocity observation for each iteration.

Each original sample is included in the filtered samples only when the above criteria are satisfied. ~~Now, we~~We refer ~~the~~to these filtered samples~~ to~~ as "common-biased samples."

2.3. *Preparation of Samples*

The original samples considered in this study were limited to companion objects detected by ~~the~~ radial-velocity observations, allowing the orbital parameters to be characterized and lower ~~limit of~~ limits to the companion ~~mass~~masses to be determined. Essentially, we selected the original samples~~ were selected~~ from those labeled "Radial Velocity" in the "detection method" column of the Extrasolar Planet Encyclopedia catalog as of the end of June 2018 (Schneider *et al*. 2011). The radial velocities of the host stars orbited by the original samples, ~~and~~as well as the orbital periods and eccentricities of the original samples, were ~~also~~ collected from the same catalog. ~~The~~ We referred to the SWEET-Cat catalog ~~was referred to~~ for the metallicity and mass of ~~the~~each host star (Santos *et al*. 2013; Sousa *et al.* 2018); this catalog presents ~~the~~ uniformly derived stellar parameters ~~of~~ for the planet-host stars. For some of the original samples that are not listed in the SWEET-Cat catalog, we used the metallicities and masses compiled in the Geneva-Copenhagen catalog (Casagrande *et al*. 2011)~~ was applied~~ and calibrated them by using regression lines for G-type and early-type stars. ~~The~~ We determined the regression lines ~~was determined~~ from the metallicity or mass ~~correlation~~correlations between the SWEET-Cat and Geneva-Copenhagen catalogs to minimize measurement biases for host-star metallicities and masses (see Figure 2). ~~Note that~~ We calibrated 41 and ~~4~~four samples ~~orbiting the~~that, respectively, orbit G-type and early-type stars ~~were, respectively, calibrated~~ in terms of the host-star metallicity. ~~Using~~Because the host-star masses were thus revised, we used the new stellar mass ~~and~~to re-calculate the lower limit ~~of~~ to the companion mass ~~was newly calculated based on~~from Equation (2~~) because the host-star masses were revised.~~).

~~The~~

As indicators of the selection effect, we extracted the measurement accuracy and term of observation ~~term~~ for the radial-velocity measurement ~~of each original sample as the indicators of the selection effect were extracted~~ from the exoplanets.org catalog~~.~~ for each original sample. According to ~~the~~ Kepler's third law, shown in Equation (1), the term of observation ~~term~~ and the host-star mass provide the upper limit ~~on~~to the semi-major axis of a detectable companion ~~with~~for each radial-velocity measurement. Using the derived maximum semi-major axis, host-star mass, and measurement accuracy, we derived the lower mass limit ~~of the~~for detectable companion ~~was derived based on~~from Equation (2).

2.4. *Boundary between Gas Giants and Neptune-like Planets*

~~Only~~

We extracted only gaseous objects ~~were extracted~~ from all the samples in the Extrasolar Planet Encyclopedia catalog to remove the impact of low-mass samples~~,~~ —such as Neptune-mass planets (gas dwarfs) and super-Earths~~, on~~—for this

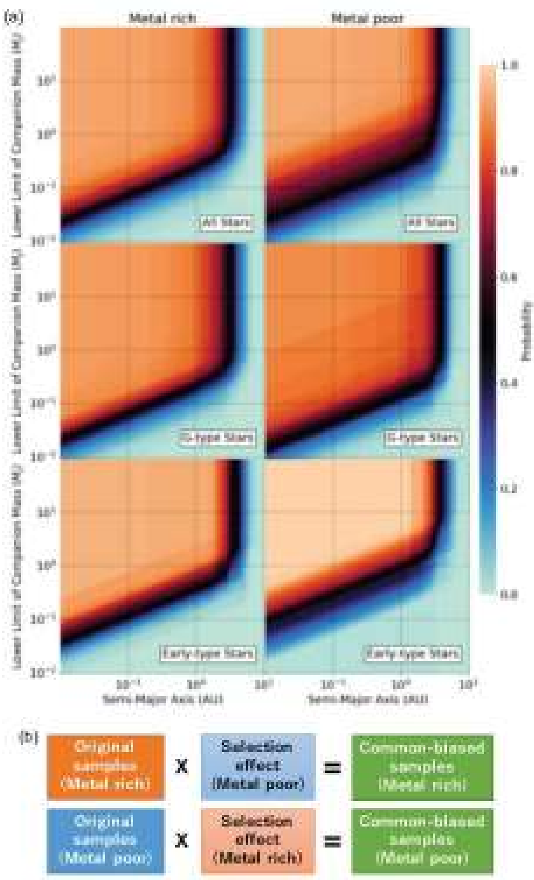

Figure 1. (a) Detection probabilities ~~of~~ for a companion ~~with~~ as derived from the radial~~-~~-velocity measurements ~~of~~for all stars (upper panel), for G-type stars (middle panel), and for early-type stars (lower panel) in ~~the~~ metal-rich (left column) and -poor regions (right column~~)~~), plotted in terms of the companion mass *vs.* the semi-major axis and ~~companion mass. 0 dex was~~. For this figure, we applied 0 dex as the metallicity boundary. ~~The~~ We defined the probability ~~was denned~~ as the fraction of the number of ~~the~~ radial~~-~~-velocity measurements that can detect a companion to the total number of ~~the~~ measurements in each metallicity region. Note that ~~the~~in this paper we define G-type and early-type stars ~~were~~, respectively, ~~denned~~ as ~~stars~~those with masses ranging from 0.8 to 1.3 ~~$M_{\odot}$~~$M_{\odot}$ and ~~ones~~those more massive than 1.3 ~~$M_{\odot}$ in this paper,~~$M_{\odot}$. (b) Procedure for equalizing the selection biases included in the original samples in the two

different metallicity regions. ~~The~~ We filtered the original metal-rich (-poor) samples ~~were additionally filtered with the selection effect constructed from~~ further using the criteria for the radial ~~-~~-velocity measurements ~~of~~ for the metal-poor (-rich) original samples. ~~The~~ We define the samples so-filtered ~~original samples were denned~~ as "common-biased samples ~~" that~~;" *i.e.*, they are biased by ~~a~~ common selection ~~effect. The~~ effects. This filtering procedure judges whether the original samples can be detected by radial ~~-~~-velocity measurements with the constructed selection effect, and the filtered samples are included in the common-biased samples only when the original samples are detectable.

Comment [Editor8]: Remark: Please check whether this edit retains your intended meaning.

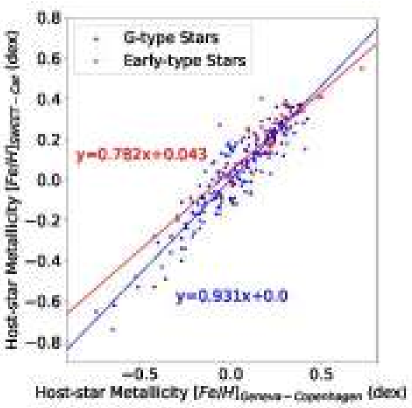

Figure 2. Metallicity correlations between the SWEET-Cat and Geneva-Copenhagen catalogs for G-type (blue) and early-type stars (red). ~~The numbers of samples in both the catalogs~~There are 271 ~~for~~ G-type stars and 58 ~~for~~ early-type stars~~,~~ common to both catalogs. The variables y and x in the linear ~~-~~-regression equations represent the host-star metallicities ~~of~~from the SWEET-Cat and Geneva-Copenhagen catalogs, respectively.

analysis. We determined the boundary mass between the ~~gaseous~~gas-giant and gas-dwarf objects from ~~a~~the perspective of both theory and observation. According to a previous study (Ida & Lin 2004a), gas-dwarf objects, ~~which~~consisting primarily ~~consist~~ of heavy-core objects such as Neptune and Uranus, have the potential to grow to the extent allowed by the core ~~-~~-building materials inside their semi-major axes. This growth occurs *via* giant impacts in the inner region of the disk after the disk gas dissipates. However, this core growth is limited by ~~the~~ scattering ~~effect of~~from the heavy core ~~increasing~~, which increases with greater ~~distances~~distance from the central star. Therefore, the mass of a gas-dwarf object reaches a maximum at the semi-major axis~~,~~ where the scattering effect begins to limit the core growth. ~~Given that~~Assuming the ratio of collision-to-ejection probabilities for the heavy core ~~is~~to be 0.1 and the core density ~~is~~to be 1 g/cm^3, ~~the~~we obtain an upper mass limit ~~of the~~for a gas-dwarf object ~~is~~ of approximately 0.1 ~~Mj~~M_J for ~~dust~~ surface densities of ~~3~~dust three times the Minimum Solar Nebulae Model value (MMSN).

From ~~a standpoint of the observation, a~~ the *Kepler* data, the boundary between gas giants and gas dwarfs ~~at~~has been found observationally to be four times the Earth's radius ~~has been observationally revealed by the Kepler data~~ (Buchhave *et al.* 2012). From the empirical planetary mass-radius relation (e.g., Bashi *et al.* 2017):

$$\frac{R_p}{R_\oplus} \propto \left(\frac{M_p}{M_\oplus}\right)^{0.55\pm0.02} , \qquad (5)$$

~~5~~

we found that the ~~boundary~~ upper limit of planetary mass is about 30 times the Earth's mass, corresponding to 0.1 ~~Mj.~~ M_J. Based on these considerations, we used 0.1 ~~Mj was applied~~ M_J in this study as the boundary mass between gas giants and gas dwarfs. ~~The numbers of~~ For this study, we considered 623 samples ~~and their~~ of gaseous planets or substellar objects belonging to 520 planetary systems ~~considered in this study are 623 and 520, respectively~~.

Comment [Editor9]: Remark: Please verify our edit here.

Comment [Editor10]: Remark: It is not clear how you found this. If we substitute R-p/R_Earth = 4 into Eq. (5), we get 12.4.

Is the difference due to the constant of proportionality? Unless this would be obvious to anyone working in your field, please clarify.

3. RESULTS

In this section, we show quantitatively ~~show~~ how different are the distributions of the orbital properties and planet masses for ~~the~~ extrasolar gaseous objects orbiting ~~the~~ metal-rich and -poor stars ~~are~~, after minimizing the impact of the radial-velocity selection effect ~~of radial velocity measurement~~ on ~~their~~ these distributions. ~~We also~~ In addition, we explore how many ~~components exit in the~~ types of extrasolar gaseous objects ~~through~~ exist by classifying the common-biased samples with ~~the~~ a Gaussian-mixture model.

3.1. *Metallicity Boundary for Common-Biased Samples*

~~We first~~

First, we determined the metallicity boundary that divides the original samples into two groups, such that the distributions of ~~planet~~ planetary mass and semi-major axis in the ~~two~~ metal-rich and -poor regions ~~are~~ differ the most ~~different, respectively, considering the selection effect~~ after taking account of the radial-velocity ~~measurements~~ selection effect, as explained in Section 2.1. Figure 3 shows the p-values derived by the two-sample Anderson-Darling test for the distributions of the semi-major axes and lower mass limits of the common-biased samples, changing the metallicity boundary from −0.7 to 0.4 dex. We iterated the calculation 1,000 times and averaged the calculated p-values ~~for~~ at each ~~divided~~ dividing point to derive the ~~mean~~ means and standard ~~deviation~~ deviations of the p-values. The minimum p-values ~~of~~ from the two-sample Anderson-Darling tests for the distributions of the semi-major ~~axis~~ axes and ~~the planet mass were~~ planetary masses are 2.4 x 10~$^{-3}$ and 3.5 x 10~$^{-5}$/4.2 x 10~$^{-5}$ at the ~~metallicity of~~ metallicities −0.04 and −0.29/−0.06 dex, respectively. Thus, we have found that the planetary distributions in the metal-rich and -poor regions do not arise from the radial-velocity selection effect ~~of the radial velocity measurements~~ but rather from the planet formation and evolution ~~. In~~ mechanism. Therefore, in this study, we used ~~applied~~ −0.05 dex as the

Comment [Editor11]: Tip: Minus Sign: The minus sign is preferred over the hyphen for indicating that values are negative.

metallicity boundary for constructing the common-biased samples, considering that the two minimum p-values are around ~~-~~−0.05 dex.

Next, as shown in Figure 4, we compared the distributions of semi-major axes and lower limits of companion mass for the common-biased sub-samples in the metal-rich and -poor regions that ~~were divided by~~we separated at the boundary metallicity of ~~-~~−0.05 dex. ~~The~~In the metal-poor region, samples with semi-major axes less than 0.3 AU are relatively lacking, and masses larger than

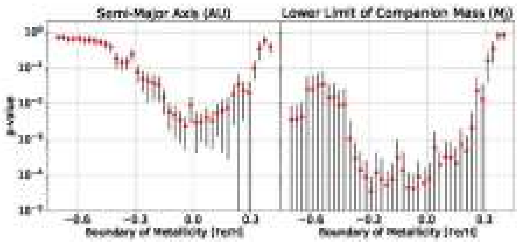

Figure 3. ~~P~~The p-values calculated *via* two-sample Anderson-Darling tests for the semi-major axis (left) and the lower limit of ~~the~~ companion mass (right) ~~of~~for the original samples, as ~~a function~~functions of the assumed metallicity boundary. The red points and black vertical bars represent the mean p-values and their standard deviations, respectively. The number of ~~the~~ calculations for each metallicity boundary is 1,000.

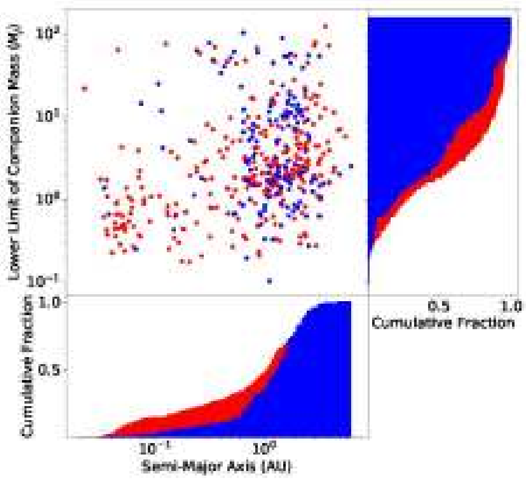

Figure 4. Distribution of semi-major axes and lower limits of companion mass for the common-biased samples (upper left) and the cumulative distributions of semi-major ~~axis~~axes (bottom) and lower ~~limit~~limits of companion mass (right). The red and blue points/bins represent the metal-rich and -poor samples, respectively. ~~An~~This figure shows one example from among the 1,000 calculations ~~was shown~~.

about 5 ~~Mj in the metal-poor region~~M_J are relatively ~~lack and excess~~abundant, compared to those in the metal-rich region~~, respectively.~~. In Section 3.3, we discuss ~~where~~ the origin of this difference between the planetary distributions in the metal-rich and -poor regions ~~comes from.~~.

3.2. —*Three*~~-~~ *Mass Regimes of Gaseous Objects*

We classified the common-biased samples selected from the 623 original ones in a diagram ~~of~~showing the companion mass *vs.* host-star metallicity~~ and companion mass with the~~, using a Gaussian~~-~~-mixture model to explore how many distinct sub-samples exist ~~in~~among the extrasolar gas giants discovered to ~~data~~date, given that each sub-sample follows a normal distribution. ~~Changing the number of the sub-samples, we~~ We evaluated each model ~~with~~using the Bayesian Information Criterion ~~and~~ while varying the number of sub-samples. In this way, we found that ~~the~~a three-component model is ~~suitable as~~ the best Gaussian~~-~~-mixture model for the common-biased samples. Figure 5 shows ~~the~~ this best~~-~~-suited model~~ for the common-biased samples.~~. The common-biased samples are divided into three ~~almost along~~ groups by the two boundary masses of 4 and 20 ~~Mj. The~~M_J. This three-component model results from a relative paucity of ~~the~~ common-biased samples in two specific regions in the diagram of companion mass *versus* host-star metallicity~~ versus companion mass; the two regions indicate gaseous objects with masses ranging~~: the mass range from 20 to 30 ~~Mj~~M_J around both the metal-rich and -poor stars and ~~those with masses ranging~~the mass range from 0.1 to 4 ~~Mj~~M_J around the metal-poor stars. ~~As a result~~Consequently, the mean metallicity of the stars hosting ~~the~~ gaseous objects ~~more~~ with masses ~~from~~between 4 ~~to~~and 20 ~~Mj~~M_J is lower than that of the samples lighter than 4 ~~Mj~~M_J, and the mean metallicity of the samples more massive than 20 ~~Mj~~M_J is much lower than those of the other two sub-samples. Thus, we ~~also~~have confirmed that the lower boundary mass is consistent with the results ~~shown~~obtained in~~ the~~ previous studies (Ribas & Miralda-Escude 2007; Santos *et al*. 2017; Schlaufman 2018).

3.3. *Planetary distributions around G- and early-type* *stars*

~~We next~~

Next, we extracted ~~the~~ sub-samples from among the common-biased samples orbiting G-type stars with masses ranging from 0.8 to 1.3 ~~M©~~$M_\odot$ and early-type stars more massive than 1.3 ~~M© from the common-biased samples~~$M_\odot$, and ~~then~~we investigated the distributions of host-star metallicities and companion masses around the two types of host~~-~~ stars. Figure 6 shows the distributions of host-star metallicities for the three substellar-mass regimes ~~of~~ for the G-type and early-type stars. Note that we have constructed the common-biased sub-samples for G-type and early-type stars ~~were constructed~~ by accounting for the selection biases for the two different spectral~~ type-~~ types of stars, as shown in the middle and lower panels of Figure 1 (a).

~~Regarding the distribution of host-star metallicity around the G-type stars, the~~

The mean metallicities ~~for~~of the G-type host-stars with gaseous samples lighter than 20 ~~Mj~~M_J are much higher than ~~that of the~~those with samples more massive than 20 ~~Mj, which almost~~M_J. This corresponds closely to ~~that~~the metallicity of the nearby G-type stars selected from the Geneva-Copenhagen catalog (Casagrande *et al.* 2011). There is also no boundary at 4 Mj in terms of the distribution of the host-star

~~metallicity.~~metallicities. While a ~~stellar~~ star-formation process such as gravitational core collapse and fragmentation of a molecular ~~clouds~~cloud (Padoan & Nordlund 2004; Hennebelle & Chabrier 2008) forms ~~the~~ gaseous objects more massive than 20 ~~Mj, the~~M_J, gaseous objects with masses ranging from 4 to 20 ~~Mj~~ M_J—as well as from 0.1 to 4 ~~Mj~~ M_J—are thought to be formed *via* core-accretion. Thus, the ~~larger~~ upper boundary ~~of~~ around 20 ~~Mj clearly~~M_J apparently reflects the upper mass limit ~~of the~~for core-accreted planets, which ~~are almost~~is approximately consistent with those ~~shown~~found in ~~the~~ previous theoretical studies (*e.g.*, Tanigawa & Ikoma 2007; Mordasini *et al.* 2009; Tanigawa & Tanaka 2016). Note that the paucity of samples more massive than 20 ~~Mj~~M_J around ~~the~~ early-type stars also seems to support ~~that the~~this upper boundary ~~corresponds to~~as the maximum mass ~~of the~~for a planetary ~~objects~~object.

In contrast, ~~regarding the distribution of host-star metallicities and companion masses around the~~for early-type stars, the mean metallicity for ~~the~~ gaseous objects with masses ranging from 4 to 20 ~~Mj~~M_J is much lower than ~~that of~~for the samples lighter than 4 ~~Mj.~~M_J. Therefore, the lower boundary mass of 4 ~~Mj in the three mass regimes indicates~~M_J seems to indicate that the distribution of ~~the~~ host-star ~~metallicity largely~~metallicities changes significantly at the 4 M_J boundary ~~of 4 Mj~~ around ~~the~~ early-type stars. ~~The~~This lower boundary also reflects a difference between the planetary~~-~~-formation processes around ~~the~~ G-type and early-type stars, ~~considering that~~since there is no boundary at 4 ~~Mj~~M_J around ~~the~~ G-type stars. In fact, although the common-biased sub-samples with masses ranging from 4 to 20 ~~Mj~~M_J orbiting ~~the~~ G-type and early-type stars ~~distribute~~are distributed in the outer region ~~than~~of the planetary system beyond 0.3 AU (Figure 4), their eccentricity distributions are ~~largely~~quite different, as shown in Figure ~~6.~~7. Note that, because we calibrated 41 and ~~2~~ two of the samples~~.~~, respectively, among the 380 G-type and 189 early-type stars ~~were calibrated~~ in terms of the host-star metallicity, ~~respectively,~~ the impact ~~of non-uniformity in the samples~~ on the distribution of host-star metallicities from non-uniformities in the samples is small.

Comment [Editor12]: Remark: Please verify our edit here.

Based on the ~~above~~ considerations above, we redefined the samples lighter than 20 ~~Mj~~M_J as planetary-mass objects and labeled the two sub-samples with masses from 0.1 to 4 ~~Mj~~M_J and from 4 to 20 ~~Mj~~M_J as "intermediate-mass planets" and "massive planets," respectively. In addition, we re-labeled the samples more massive than 20 ~~Mj are labeled~~M_J as "brown~~-~~ dwarfs." Note that the boundary between plan-etary~~-~~-mass and brown~~-~~-dwarf objects established by the deuterium-burning minimum mass of around 10 ~~Mj~~M_J is semantic (Chabrier *et al.* 2014); this boundary has no physical meaning from the evolutionary perspective~~ object evolution~~.

4. DISCUSSION

In this section, ~~we~~ first, we discuss the formation process of ~~the~~ intermediate-mass and massive planets orbiting

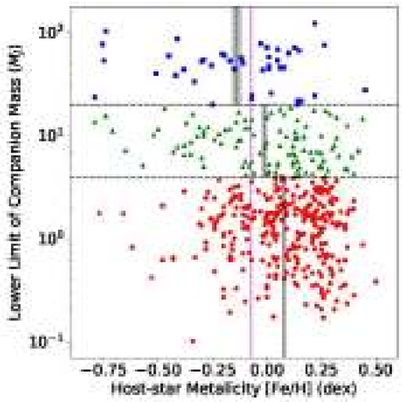

Figure 5. Distribution of ~~host-star metallicities and~~ the lower limits of companion mass ~~for~~as a function of host-star metallicity for the three common-biased sub-samples classified by the best Gaussian~~-~~-mixture model. The different symbols ~~of~~ (square, triangle, and circle) represent the classified sub-samples. The three colors of the samples correspond to three~~-~~ mass regimes ~~with~~separated by the two boundary masses ~~of~~ 4 and 20 ~~Mj~~M_J, which are shown by the horizontal long-dashed lines. The vertical short dashed line and gray region in each mass regime represent the mean metallicity and its standard deviation over 1000 iterations, respectively. ~~The~~This distribution of the lower limit of companion mass of the samples ~~in terms of~~*vs.* host-star metallicity ~~and lower limit of companion mass~~ shows ~~an~~one example from among the 1000 calculations. The magenta dashed line ~~and region, respectively,~~ shows the mean metallicity ~~and its standard error~~ for all the samples in the Geneva-Copenhagen catalog, where we converted the mean metallicity ~~was converted with~~using the linear regression between the samples in the SWEET-Cat and that ~~catalogs~~catalog. ~~the~~

Comment [Editor13]: Remark: We have deleted the phrase “and region” because we do not see a magenta region in this figure. Please check and revise as applicable.

G-type stars, comparing the mass distribution with that predicted by the core~~-~~-accretion model. ~~We next~~Then, we focus on the distributions of masses and eccentricities for the intermediate-mass and massive planets orbiting ~~the~~ early-type stars. We finally ~~show~~provide an ~~entire view~~overview of the extrasolar gaseous objects discovered so far ~~from a standard point~~in the context of the two ~~planetary~~ planet-formation scenarios.

4.1. *Planetary Formation ~~Process~~Processes around G-Type Stars*

We compared the intermediate-mass and massive planets with ~~the~~ simulation data generated by Mordasini *et al.* (2012~~) that~~), who performed ~~a~~ population synthesis around a 1 ~~M©~~ $M_\odot$ star within the framework of the core~~-~~-accretion model, including planet growth and migration ~~through~~ caused by planet-disk ~~interaction.~~interactions. The upper ~~panel~~panels of Figure 8 ~~shows~~show the distributions of ~~semi-major axes and~~ masses for the common-biased intermediate-mass and massive planets and of the simulation samples ~~in~~as functions of the semi-major axes for both the metal-rich and -poor regions. ~~The distribution of semi~~

These distributions

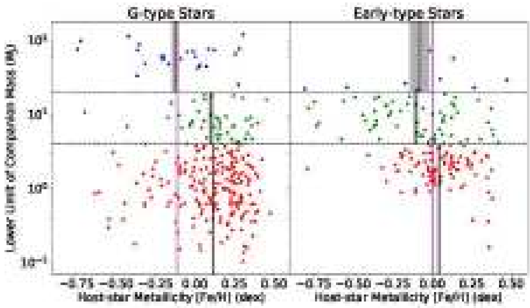

Figure 6. Distributions of companion masses as functions of the host-star metallicities ~~and companion masses~~ for the common-biased samples orbiting G-type stars with masses ranging from 0.8 to 1.3 ~~$M_\odot$~~$M_\odot$ (left) and orbiting early-type stars with masses ~~more massive~~greater than 1.3 ~~$M_\odot$~~$M_\odot$ (right). The symbols are same as those in Figure 5. ~~The~~We constructed the common-biased samples for G-type and early-type stars ~~were constructed~~ by compensating for the radial-velocity selection effects ~~of the radial velocity measurements~~ for the two spectral ~~type~~ types of stars, as shown in the middle and lower panels of Figure 1~~,~~ (a).

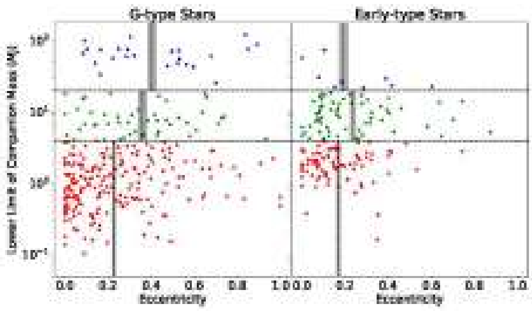

Figure 7. Distributions of companion masses as functions of the eccentricities ~~and masses~~ for the common-biased samples orbiting G-type (left) and early-type stars (right). The symbols and lines are same as those in Figure 5.

~~major axes and masses for the intermediate-mass and massive planets around G-type stars~~ are ~~almost~~approximately consistent with that ~~for~~from the ~~simulation samples.~~simulations. In fact, as shown in the lower panel of Figure 8, the mean masses for the ~~observation~~observations of planets around G-type stars ~~and~~agree well with the simulation samples ~~have a good agreement~~ over the entire ~~metallicity region.~~range of metallicities. Note that we filtered the simulation samples ~~were also filtered by both~~for the selection effects ~~of~~ for both metal-rich and -poor regions, and we restricted the observational samples ~~were restricted to the~~to intermediate-mass and massive planets orbiting host stars with masses ranging from 0.8 to 1.3 ~~$M_\odot$~~$M_\odot$.

~~An increase~~

The increases in the eccentricities of the massive planets orbiting G-type stars, shown in Figure 7, can ~~be~~ also be explained by the following two models~~ that were expanded from~~, which are extensions of the core~~-~~-accretion model. One ~~is~~extension involves planet-disk ~~interaction~~interactions at the Lindblad and co-rotation resonances prior to gas dissipation (*e.g.*, Goldreich & Sari 2003). According to the numerical simulations performed by Kley & Dirksen (2006), the minimum ~~planet~~planetary mass ~~for changing~~necessary to change the disk gas into a high~~-~~-eccentricity state is 3 ~~Mj~~M_J for ~~the~~a viscous coefficient of 10~^{5}~~, which~~. This is ~~almost~~approximately consistent with the boundary between the intermediate-mass and massive planets. ~~Another is~~The second extension involves dynamical ~~instability~~instabilities induced by two closely separated gas giants ~~and~~ or by three gas giants, so~~-~~-called "gravitational planet-planet ~~interaction~~interactions" (*e.g.*, Ida *et al*. 2013). The dynamical instability produces a gas giant with an eccentric orbit in the outer region of the planetary system and a circular hot Jupiter in the inner region through tidal circularization (*e.g.*, Rasio & Ford 1996). In fact, ~~a~~we confirm the paucity of ~~the~~ intermediate-mass planets ~~that locate~~located within 0.1 AU around ~~the~~ metal-poor G-type stars~~ was confirmed~~; the gravitational planet-planet interaction is ~~thoughg~~thought to occur only around ~~the~~ metal-rich G-type stars. ~~The previous~~Previous observations have also confirmed that hot Jupiters ~~orbit~~ only ~~the~~orbit metal-rich G-type stars (Dawson & Murray-Clay 2013; Adibekyan *et al*. 2013).

Thus, the distributions of masses and eccentricities for the intermediate-mass and massive planets orbiting G-type stars can be explained naturally ~~explained~~ by the core~~-~~-accretion model. Their distributions support the conclusion that the upper mass limit ~~of the~~for core-accreted planets is around 20 ~~Mj~~M_J.

4.2. *Planetary Formation ~~Process~~Processes around Early-Type Stars*

~~Considering~~

Because the mean host-star metallicity for ~~the~~ intermediate-mass planets orbiting early-type stars is relatively higher than that for ~~the~~ massive planets, the intermediate-mass planets are thought to be formed by core accretion. In contrast, the massive planets around early-type stars seem to ~~preferentially~~ orbit ~~the~~ metal-poor stars~~.~~ preferentially. Note that the mean value of the nearby early-type stars extracted from the Geneva-Copenhagen Catalog may be higher than the true value because of a systematic offset between the Geneva-Copenhagen and SWEET-Cat catalogs. In addition, the ~~distribution~~distributions of semi-major axes and masses for the massive planets around early-type stars ~~is~~are not consistent with ~~that for~~ the simulation samples; there is an excess of ~~the~~ massive planets orbiting metal-poor stars, and most of the planets ~~locally distribute~~are distributed in the transition region between 1 and 3 AU, ~~in which the~~where there is a paucity of simulation samples~~ are paucity~~. The excess of massive planets orbiting metal-poor early-type stars differs from that expected form the core~~-~~-accretion

Comment [Editor14]: Remark: It is not clear how this conclusion can be drawn from Fig. 6. Unless this would be immediately obvious to anyone working in your field, please clarify.

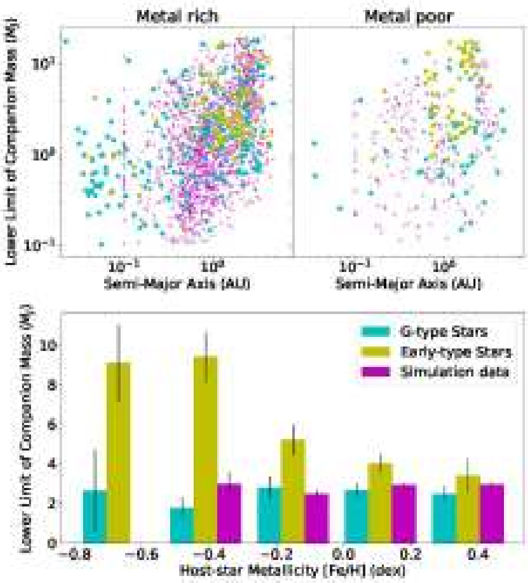

Figure 8. *Top:* Distributions of ~~semi-major axes and~~ the lower limit of companion masses as a function of semi-major axis for the common-biased samples with masses less than 20 ~~Mj~~M_J orbiting G-type stars~~ with~~. The G-star masses ~~ranging~~range from 0.8 to 1.3 ~~M⊙~~$M_\odot$ (cyan dots~~)~~), and the early-type stars are more massive than 1.3 ~~M⊙~~$M_\odot$ (yellow dots~~) and the~~). The simulation samples ~~with~~generated by Mordasini *et al.* (2012) have companion masses ranging from 0.1 to 20 ~~Mj~~M_J (purple dots~~) generated by Mordasini et al. (2012) in the~~). The metal-rich ~~(upper left)~~ and -poor regions ~~(~~are shown in the upper left and upper right~~)~~. panels of the figure, respectively. *Bottom:* Histograms of mean masses ~~for~~from the simulation samples (purple bars) and from the common-biased samples with masses less than 20 ~~Mj~~M_J orbiting G-type stars (cyan bars) and early-type stars (yellow bars).

formation theory ~~in terms of~~regarding the following two points~~.~~: (1) While more-massive planets are ~~likely~~expected to be formed around more metal-rich stars (Mordasini *et al.* 2012), the mean masses for the intermediate-mass and massive planets orbiting early-type stars clearly ~~increases~~increase as the metallicity decreases (Figure 8). (2) In addition, although ~~a continuous decrease in~~ the mass function ~~of~~for massive planets is theoretically predicted to exhibit a continuous decrease (Mordasini *et al.* 2009), the ~~observation~~observational samples orbiting metal-poor early-type stars ~~are clustered~~cluster around 4 and 10 ~~Mj~~M_J (Figure 8). The eccentricities of the massive planets ~~orbiting~~that orbit early-type stars also differ from those around the G-type stars (Figure 7); the eccentricities of the massive planets around the early-type stars do not seem to be enhanced ~~through the~~by planet-disk ~~interaction~~interactions prior to gas dissipation

~~and~~or by gravitational planet-planet ~~interaction.~~interactions. Thus, the distributions of masses and eccentricities for the massive planets orbiting early-type stars are unlikely to be explained by the bottom-up models.

An explanation for the excess of massive planets orbiting metal-poor stars is that the disk instability acts in the vicinity of metal-poor stars, because a lower mass limit applies ~~for~~ to planets formed *via* the disk-instability mechanism ~~(~~[*i.e.,* corresponding roughly to ~~an order of~~ the Jeans mass (Matsuo *et al.* 2007; Mayer 2010~~)). As a result~~)]. Consequently, a sharp increase appears in the planetary mass function around 4 ~~Mj.~~M_J. It is also generally accepted that planet formation due to the disk instability tends to occur in the vicinity of metal-poor stars, because the cooling timescale in the disk mid-plane is reduced owing to the low disk opacity (Cai *et al.* 2006; Durisen *et al.* 2007). The low eccentricities of the massive planets orbiting ~~the~~ early-type stars are also consistent with ~~the~~ numerical simulations (Mayer *et al.* 2004; Mayer 2010; Boss 2011) and with the eccentricities of the four gas giants orbiting HR8799, an A-type star, (Wertz *et al.* 2017). Note that the four gas giants are located in ~~a~~ the region beyond the core-accretion model (see Figure 9~~.~~).

4.3. *Planetary Formation Scenarios*

Based on the ~~above~~ considerations above, we have compared the distribution of companion masses as a function of the host-star metallicities ~~and companion masses~~ for the common-biased samples selected from the 623 original ones with the planet-formation regions expected from the core-accretion and disk-instability models for ~~the~~ G-type and early-type stars (Figure 9). ~~The scarce~~Sparsely populated regions ~~appear in terms~~ of companion mass~~, those at~~ occur between 0.1 ~~to~~ and 0.~~3 Mj~~3M_J and between 20 ~~to~~ and 30 ~~Mj~~M_J around G-type stars and ~~those at~~between 0.1 ~~to~~ and 1 ~~Mj~~M_J and ~~in~~ larger than 20 ~~Mj~~M_J around early-type stars. The lack of ~~the~~ lighter planets orbiting G-type and early-type stars arises from ~~the~~ rapid gas accretion onto the core. In contrast, the ~~lack~~gap in the distribution of ~~the~~ massive companions around G-type stars ~~represents a~~ corresponds to the gap between binary-star and planet formation. In addition, ~~few~~ the paucity of brown dwarfs around ~~the~~ early-type stars may support the conclusion that the boundary mass of ~~around~~about 20 ~~Mj~~M_J corresponds to the maximum mass of a planetary ~~objects.~~object. Thus, the upper and lower ~~and upper~~ boundaries of the two regions appear to reflect the upper and lower ~~and upper~~ mass limits ~~of~~for extrasolar gaseous objects that are formed by the ~~planetary~~ two planet-formation processes~~, respectively.~~. In fact, ~~the~~this upper mass limit is ~~almost~~approximately consistent with ~~the~~ theoretical expectations (Tanigawa & Ikoma 2007; Mordasini *et al.* 2009; Tanigawa & Tanaka 2016).

Comment [Editor15]: Remark: Could this not also result from selection effects? The lower masses are harder to detect.

While the intermediate-mass and massive planets orbiting G-type stars can be explained by the core~~-~~-accretion model, the ~~excess~~abundance of massive planets around early-type stars is likely to be explained not by ~~the~~a bottom-up scenario but instead by ~~the~~a top-down ~~one~~mechanism such as gravitational instability. ~~The previous~~Previous observational studies ~~on dual~~of the two

~~planetary~~ planet-formation scenarios (Ribas & Miralda-Escude 2007; Santos *et al*. 2017; Schlaufman 2018) ~~showed~~have shown that ~~there exists~~ a boundary mass of 4 to 10 ~~MJ~~M_J exists in the diagram of host-star metallicities and masses for gaseous objects and ~~mentioned~~have pointed out that ~~the~~this boundary reflects the transition between the two ~~planetary formations;~~planet-formation processes; *i.e.*, the upper limit ~~of the~~ for core-accreted planets is around 4 ~~MJ.~~M_J. However, we have found that the boundary ~~of~~at 4 M_J ~~reflects~~instead seems to reflect a population that is likely to ~~be~~have been formed *via* the disk instability ~~and expected~~, while we expect that planets with masses up to 20~~-~~–30 M_J can be formed continuously ~~formed~~ by core-accretion around G-type stars ~~stars.~~.

REFERENCES

Adibekyan, V. Z., Figueira, P., Santos, N. C., et al. 2013,
A&A, 560, A51 Bashi, D., Helled, R., Zucker, S., & Mordasini, C. 2017,
A&A, 604, A83 Boss, A. P. 1997, Science, 276, 1836 Boss, A. P. 2002, ApJL, 567, L149 Boss, A. P. 2011, ApJ, 731, 74
Buchhave, L. A., Latham, D. W., Johansen, A., et al. 2012,
Nature, 486, 375 Cai, K., Durisen, R. H., Michael, S., et al. 2006, ApJL, 636, L149
Casagrande, L., Schonrich, R., Asplund, M., et al. 2011,
A&A, 530, A138
Chabrier, G., Johansen, A., Janson, M., & Rafikov, R.
2014, Protostars and Planets VI, 619 Chiang, E. I., Fischer, D., & Thommes, E. 2002, ApJL,
564, L105
Dawson, R. I., & Murray-Clay, R. A. 2013, ApJL, 767, L24 Dodson-Robinson, S. E., Veras, D., Ford, E. B., &
Beichman, C. A. 2009, ApJ, 707, 79 Dupuy, T. J., & Liu, M. C. 2011, ApJ, 733, 122
Durisen, R. H., Reipurth, V. Jewitt, Keil, K., et al. 2007, Univ. of Arizona Press, Tucson 951, 607-622
Fischer, D. A., & Valenti, J. 2005, ApJ, 622, 1102 Girardi, L., Bressan, A., Bertelli, G., & Chiosi, C. 2000,
A&AS, 141, 371 Goldreich, P., & Sari, R. 2003, ApJ, 585, 1024
Hayashi, C., Nakazawa, K., & Nakagawa, Y. 1985, Protostars and Planets II, 1100
Hennebelle, P., & Chabrier, G. 2008, ApJ, 684, 395
Hidalgo, S. L., Pietrinferni, A., Cassisi, S., et al. 2018, ApJ,
856, 125
Ida, S., & Lin, D. N. C. 2004a, ApJ, 604, 388 Ida, S., & Lin, D. N. C. 2004b, ApJ, 616, 567 Ida, S., Lin, D. N. C., & Nagasawa, M. 2013, ApJ, 775, 42

Kalas, P., Graham, J. R., Chiang, E., et al. 2008, Science,
322, 1345
Kley, W., & Dirksen, G. 2006, A&A, 447, 369 Kuiper, G. P. 1951, Proceedings of the National Academy of Science, 37, 1
Lagrange, A.-M., Bonnefoy, M., Chauvin, G., et al. 2010,
Science, 329, 57 Lambrechts, M., & Johansen, A. 2012, A&A, 544, A32 Lee, K. J., Guillemot, L., Yue, Y. L., Kramer, M., &
Champion, D. J. 2012, MNRAS, 424, 2832 Ma, B., & Ge, J. 2014, MNRAS, 439, 2781
Marois, C., Macintosh, B., Barman, T., et al. 2008, Science,
322, 1348
Matsuo, T., Shibai, H., Ootsubo, T., & Tamura, M. 2007,
ApJ, 662, 1282
Mayor, M., & Queloz, D. 1995, Nature, 378, 355 Mayer, L., Quinn, T., Wadsley, J., & Stadel, J. 2002,
Science, 298, 1756 Mayer, L., Quinn, T., Wadsley, J., & Stadel, J. 2004, ApJ, 609, 1045
Mayer, L., Lufkin, G., Quinn, T., & Wadsley, J. 2007, ApJL, 661, L77
Mayer, L. 2010, Formation via Disk Instability. Formation and Evolution of Exoplanets, by Barns, R. (eds.) Wiley,
71-99
Mayor, M., Marmier, M., Lovis, C., et al. 2011,
arXiv:1109.2497 Mizuno, H. 1980, Progress of Theoretical Physics, 64, 544
Mordasini, C., Alibert, Y., Benz, W., & Naef, D. 2009,
A&A, 501, 1161 Mordasini, C., Alibert, Y., Benz, W., Klahr, H., &
Henning, T. 2012, A&A, 541, A97 Ormel, C. W., & Klahr, H. H. 2010, A&A, 520, A43
Padoan, N., & Nordlund, A. 2010, ApJ, 617, 559
Perri, F., & Cameron, A. G. W. 1974, Icarus, 22, 416
Pollack, J. B., Hubickyj, O., Bodenheimer, P., et al. 1996,
Icarus, 124, 62 Rasio, F. A., & Ford, E. B. 1996, Science, 274, 954
Ribas, I., & Miralda-Escude, J. 2007, A&A, 464, 779 Santos, N. C., Israelian, G., Mayor, M., Rebolo, R., &
Udry, S. 2003, A&A, 398, 363 Santos, N. C., Israelian, G., & Mayor, M. 2004, A&A, 415, 1153
Santos, N. C., Sousa, S. G., Mortier, A., et al. 2013, A&A, 556, A150

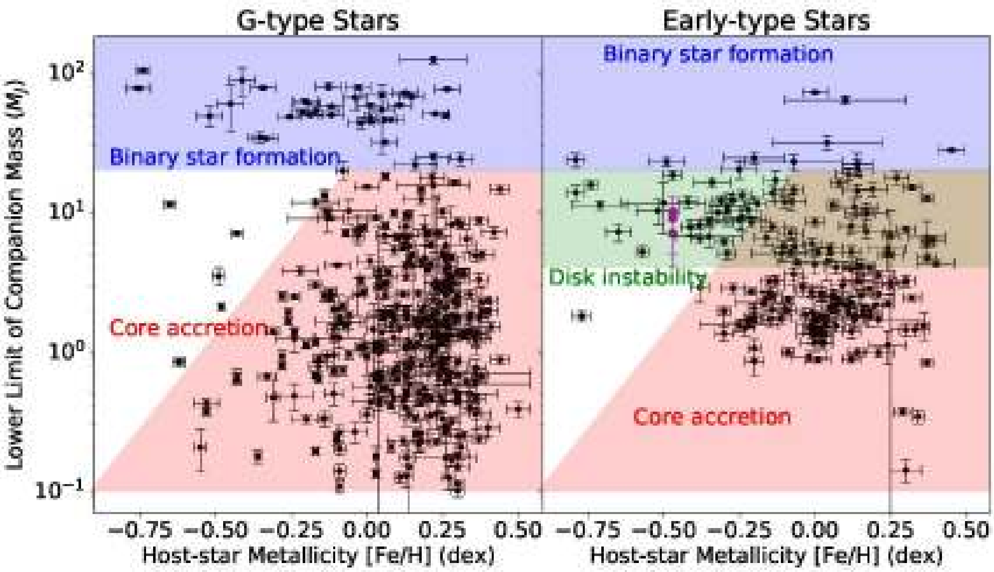

Figure 9. Distributions of companion masses as functions of the host-star metallicities ~~and companion masses~~ for the common ~~biases~~-biased samples orbiting G-type stars (left) and early-type stars (right). The common-biased samples (black dots) and the four planets orbiting HR 8799 (purple dots) ~~were~~are compared with expectations from the core~~-~~-accretion and disk~~-~~-instability theories ~~in terms of host-star metallicities and planetary mass distributions.~~. The red, green, and blue regions, respectively, indicate where ~~the~~ objects can be formed by core accretion~~,~~ or by disk instability and where binary~~-~~-star formation~~, respectively.~~ occurs. The black error bars represent ~~the~~ 1 ~~σ~~σ measurement errors. ~~The~~ We have assumed the dependence of the maximum mass ~~of the core-accreted planets~~ on the disk metallicity for core-accreted planets to be same around early-type stars ~~was assumed to be same~~ as ~~that~~ around G-type stars, which ~~was derived~~dependence we obtained from the population synthesis performed by Mordasini *et al.* (2012).

Santos, N. C., Adibekyan, V., Figueira, P., et al. 2017,

A&A, 603, A30 Schlaufman, K. C. 2018, ApJ, 853, 37 Schneider, J., Dedieu, C., Le Sidaner, P., Savalle, R., &

Zolotukhin, I. 2011, A&A, 532, A79 Sousa, S. G., Santos, N. C., Mayor, M., et al. 2008, A&A, 487, 373

Sousa, S. G., Santos, N. C., Israelian, G., et al. 2011, A&A, 533, A141

Sousa, S. G., Adibekyan, V., Delgado-Mena, E., et al. 2018,

A&A, 620, A58 Tanigawa, T., & Ikoma, M. 2007, ApJ, 667, 557 Tanigawa, T., & Tanaka, H. 2016, ApJ, 823, 48 Torres, G., Winn, J. N., & Holman, M. J. 2008, ApJ, 677,
1324
Wang, J., & Fischer, D. A. 2015, AJ, 149, 14 Wertz, O., Absil, O., Gomez Gonzalez, C. A., et al. 2017, A&A, 598, A83